DOI 10.1007/s11062-024-09947-5
Neurophysiology, Vol. 54, Nos. 3–4, May, 2022

A "Thermodynamic" Model of Central Commands for Two-Joint Arm Movements in Humans

A. I. Kostyukov,[1] A. V. Gorkovenko,[1] A. V. Maznychenko,[1,2] and I. V. Sokolowska[2]

Received December 27, 2022

Previously, we proposed a "thermodynamic" model (T-model) in an attempt to analyze temporal dynamics of the central commands (CCs) coming to the muscles in the course of forelimb movements in humans. The model used electromyography (EMG) data and was tested on a simplified geometric simulation of a human arm with a fixed shoulder joint in the case of parafrontal hand movements under the action of tangential loads. The T-model is based on equations that determine the relationship between infinitesimal changes in the muscle force and length, which, by analogy with the principles of classic thermodynamics, are taken as exact differentials. Thus, our study represents the further development of the T-model, taking into account the CCs coming to the elbow joint muscles, belonging to the subject with known biomechanical parameters of his arm identified via magnetic resonance imaging (MRI). When considering circular planar movements of the subject's hand against the background of tangential loads, symmetrical sinusoidal force waves develop in the muscles, and the CC waves acquire asymmetric shapes. The proposed method of the equalization/normalization procedure in the T-model allows us to formally consider the inverse transformation of the symmetric force waves into asymmetric CCs, which are the root cause of force generation. This approach was found to be quite effective in describing hysteresis differences of the CCs related to oppositely directed test movements. To analyze these differences using the T-model, we propose a method using multiplicative or additive correction terms to be applied to the muscle stiffness, or force velocity, respectively. The further development of the T-model is discussed concerning the real experimental practice.

Keywords: modeling, thermodynamics, human forelimb, motor control, central commands, two-joint movements, muscle contraction, electromyogram (EMG)

INTRODUCTION

General formulation of the problem. Despite the significantly increased experimental and technical capabilities in the studies of targeted human movements, it becomes clear that a significant increase in the number of channels for recording electrophysiological and biomechanical information in the experiment in many cases may encounter difficulties in its subsequent adequate processing and analysis. The information about the activity of a number of muscles belonging to the same or different joints or even to different limbs is closely connected with the problem of redundancy of the motor control system introduced by Bernstein in his hierarchical theory of voluntary movement control [1]. To manage this problem for the analysis of purposeful human movements, Bernstein introduced a simplifying concept of "synergy", which can be considered an ability of the CNS to diminish motor redundancy by reducing the degrees of freedom in the movement programs. Computational algorithms have been developed to evaluate the efficiency of motor control using the following algorithms, (1) principal component analysis, (2) independent component analysis, (3) factor analysis, (4) nonnegative matrix factorization, and others [2–4]. Several review papers have focused on the problems of movement control using a limited number of muscle synergies [7, 8].

The stability of synergies in motor actions convincingly confirms the existence of such a well-defined concept of human movement control, and this primarily concerns the movements of the upper limbs [9, 10]. Muscle synergy is likely capable

[1] Department of Movement Physiology, Bogomolets Institute of Physiology, National Academy of Sciences of Ukraine, Kyiv, Ukraine.
[2] Department of Physical Education, Gdansk University of Physical Education and Sport, Gdansk, Poland.
Correspondence should be addressed to A. I. Kostyukov (e-mail kostyuko@biph.kiev.ua).

of reconstructing muscle activity during virtual arm spatial movements or force generation tasks, and synergy models can sometimes describe the electromyography (EMG) data satisfactorily [11]. However, a striking similarity was recently found in the activity patterns of close synergists during two-joint arm movements [12–17]. With the help of graphic models, linear and circular two-joint movements were modeled for a particular case of tangential end-point loads [13], which made it possible to identify power synergies in the muscles of the proximal and distal joints for these types of movements.

Compared to the simplified hinge joints used to model arm movements, synovial joints not only show isolated rotations but are also capable of exhibiting some displacement movements. The amplitudes of translational movements in the shoulder joint are known to be capable of reaching several centimeters during large-scale movements; hand segments also cannot be correctly represented as rigid bodies fixed at a certain point [18]. In any case, accurate knowledge of the main anatomical parameters of the muscles and joints involved in the studied movement seems to be highly important for increasing the accuracy of the quantitative analysis of the real movements. To take a real step in this direction, the spatial copies of the arm bones of one subject who participated in the experiments were created using 3D printing [19]. The places of origin and attachment of the main muscles of the elbow and shoulder joints were directly determined by the prints; this, together with the determination of the exact distances between the elbow and shoulder joint axes, made it possible to evaluate the shoulders of the force moments, the moments *per se*, as well as force and length changes in the real test movements [17]. The respective EMG records and force and length trajectories, which were presented in the aforementioned study, have been used in the present modeling.

The patterns of averaged EMGs were analyzed during two different types of hand movements within the horizontal plane, the linear parafrontal [12] and the circular [16, 17], performed under external loads oriented in the tangential direction. In these studies, distinctive profiles of the related EMG activity were observed. Such problems demonstrated clear hysteresis regarding the forces acting on the muscles. For the linear parafrontal movements, the so-called "thermodynamic" model (T-model) was created [14]; this model tried to predict a nonlinear functional interdependence of the three basic parameters defining the muscle state, namely E (intensity of the efferent activity), F (muscle force), and L (muscle length). The T-model included the time-dependent integration of the equations defining the interrelations between infinitesimal changes in the preceding parameters. By inducing an additional parameter, the hysteresis weight, the T-model explained qualitatively the presence of the hysteresis effects in EMG records observed in the course of real movements of the arm. However, the model [14] was based on a simplified geometry of the muscles and bones that make up the human arm; so, it could take into account only some qualitative effects in the CC formation.

The present study is aimed at the further development of the T-model using EMG recordings in real test movements [17], while the corresponding mechanical parameters of the muscle state in these experiments were also estimated quite accurately [19]. Using the MRI method to identify the parameters, an accurate planar model of the subject's hand was created, which made it possible not only to assess changes in the muscle lengths during test movements, but also to evaluate time profiles of the generated forces. The significance of cyclic test movements for the analysis of signal transformations lies in the cyclic forms of muscle forces, which makes it possible to compare ascending and descending parts of the CCs; in addition, a change in the movement direction makes it possible to compare reactions of the muscles to changes of opposite directions in the muscle length, allowing us to adequately analyze the hysteresis effects of active muscle contractions.

Hypothesis. The T-model allows one to evaluate the functional interdependence of the main parameters that determine the state of the muscles during movements of the human hand, namely the EMG intensity, muscle length, and generated force. The T-model is based on a time-dependent integration of the equations defining interrelations between the infinitesimal changes in the aforementioned parameters, which are assumed to be exact differentials. The model has been tested using data obtained earlier in the experiments with recording EMGs from muscles of the elbow and shoulder during circular movements of the hand simultaneously with production of a force in the tangential direction [17]. The T-model is assumed to be useful for the analysis of voluntary movements when it is possible to estimate the intensity of

activation of the studied muscles using EMG methods; however, the biomechanical status of these muscles is not fully known.

METHODS

Study design. We used several experimental records from our previous study [17], where the respective methods were described in detail. Under the conditions of our tests, surface EMGs recorded from the upper limb muscles and subjected to full-wave rectification and low-frequency filtering could be considered adequate analogs of the CCs coming from the upper CNS structures to the motoneurons of these muscles. From one participant, we obtained precise data on the geometry of the musculoskeletal system of the upper limb revealed by MRI followed by 3D printing of the right arm bones [19]. The motor tests consisted of circular movements of the right hand of the subject within a plane passing through the shoulder joint. The movements were completely imposed on the subject by a robotic-mechatronic device according to the passive movement program; in parallel, with the help of a visual biofeedback system, the subject produced a force by pressing a handle of the device for measuring the force vector installed on the mobile platform of the mechatronic apparatus with his hand. The force was created in the visual biofeedback mode according to the active movement program, which consisted of creating a force vector of the constant amplitude and direction, changing tangentially with respect to the movement trajectory.

A previous description of the T-model. A T-model of CCs coming to the muscles during a movement was presented in our previous paper [14]. The study considered certain elements modeling nonlinear macrocharacteristics of the muscle contractions based on experiments with a classic nerve-muscle preparation [20]. This approach was based on the reconstruction of the nonlinear surface describing the muscle force F as a function of the two variables, E (intensity of the arriving efferent activity, i.e., of the central command, CC), and L (muscle length). Two sets of the "quasi-static" characteristics, $F(E|L=const)$ and $F(L|E=const)$, were used to define the two sets of mutually perpendicular sections of the F surface. Under experimental conditions, recording of the characteristics is carried out during slow linear changes in one of the controlled input parameters (E, L), when another one is fixed at various consecutively changed levels $L_i = i \cdot \Delta L$ and $E_j = j \cdot \Delta E$, where ΔL and ΔE represent the selected parameter discretization levels; $i, j = 0, 1, 2, \ldots$. The T-model in the aforementioned study [14] was based on Eq. (1) presented in the next paragraph; however, the consideration took into account a rough geometric diagram of the muscles and bones of the hand. The model analyzed changes in the length and force of the muscles during a presumable parafrontal rectilinear movement of the hand against the action of an externally applied tangential force. In the present study, we tried to model functional relationships between the EMG intensities recorded from the muscles and the evaluated mechanical parameters of contraction [17].

Computer simulations. Calculations and graphic plotting were performed using Origin 2018 software (OriginLab Corp., MA, USA). All tests within the T-model are based on the relevant experimental records described previously. This software was also used to check out the Gaussian fit of the relevant experimental relationships.

RESULTS

A general formulation of the T-model. First, we considered elements that must be applied in modeling the nonlinear macrocharacteristics of muscle contractions based on the experiments with a classic nerve-muscle preparation; details of this approach and corresponding experiments were described earlier [20, 21]. This approach is based on the reconstruction of a nonlinear surface representing equilibrium positions of the muscle force F as a function of two independent variables, E, the intensity of efferent activity (or a CC analog) and L, the muscle length. The nonlinear surface $F(E, L)$ is, therefore, defined by two sets of static characteristics, $F(E|L_i=const)$ and $F(L|E_j=const)$, thus representing two sets of mutually perpendicular sections of the force surface. In real experiments, the characteristics could be recorded during slow linear changes in one of the input parameters, either E or L, when another parameter is fixed at one of the consecutive discrete levels, $L_i = i \cdot \Delta L = const$ and $E_j = j \cdot \Delta E = const$, where ΔL and ΔE are levels of discretization of the arguments, $i, j = 0, 1, 2, \ldots$. The following functional dependency is used to define infinitesimal muscle force changes along any pathway passing the force surface $F(E, L)$ via the

respective independent changes of arguments:

$$dF = \left(\frac{\partial F}{\partial E}\right)_L dE + \left(\frac{\partial F}{\partial L}\right)_E dL \cdot \quad (1)$$

Equation (1) provides a procedure for linear approximation of a nonlinear surface *F(E, L)* within its domain of definition: $0<E<E_{max}$; $L_{min}<L<L_{max}$, restricted by appropriate natural physiological and anatomical limitations. At any point of the *F(E, L)* surface, the partial derivatives $\left(\frac{\partial F}{\partial E}\right)_L$ and $\left(\frac{\partial F}{\partial L}\right)_E$ are defined by the respective mutually perpendicular sections of the force surface. By analogy with the formalism used in thermodynamics, we will further consider the differentials *dF*, *dE*, and *dL* in Eq. (1) as exact differentials [22]. Therefore, this equation can also be considered the basis for describing active muscle contractions within the framework of the T-model presented earlier [14].

In general, the quasistatic characteristics are nonlinear; therefore, the partial derivatives $\left(\frac{\partial F}{\partial E}\right)_L$ and $\left(\frac{\partial F}{\partial L}\right)_E$ can be essentially changed at various places within the working space *(E, L)*. Moreover, both characteristics are crucially dependent on the direction of changes in the input variables, thus demonstrating powerful hysteresis effects; the latter represent an expression of the principally nonlinear properties of muscle contraction [21, 23].

Because our goal is to analyze temporal changes in the CCs providing a given movement, Eq. (1) may be transformed as follows:

$$dE = \left(\frac{\partial F}{\partial E}\right)_L^{-1} dF - \left(\frac{\partial F}{\partial E}\right)_L^{-1} \left(\frac{\partial F}{\partial L}\right)_E dL . \quad (2)$$

For partial derivatives, which define the relationships between functions that can be represented by exact differentials, there are the reciprocity relationships showing that the inverse partial derivative is equal to its reciprocal [22]. Therefore, an equality between the derivatives $\left(\frac{\partial F}{\partial E}\right)_L^{-1}$ and $\left(\frac{\partial E}{\partial F}\right)_L$ does exist, and Eq. (2) is equivalent to the following expression:

$$dE = \left(\frac{\partial E}{\partial F}\right)_L \left[dF - \left(\frac{\partial F}{\partial L}\right)_E dL\right]. \quad (3)$$

Normalization of the data of real movement tests. In the subsequent, we will further consider cyclic movements of the hands, in which forces acting on the muscles are waves resembling the symmetrical positive parts of sinusoids. Figure 1A demonstrates the responses of the *biceps brachii* (*BicBr*) muscle registered in the experiments with circular movements of the right arm within a plane passing through the shoulder joint [17]. The movements were produced by the robotic-mechatronic device in accordance with the *passive movement program*; in parallel, using the visual biofeedback system, the subject created an effort by pushing his hand on the handle of the force vector-measuring device installed vertically at the moving platform of the mechatronic apparatus. The effort was created in the visual biofeedback regimen in accordance with the *active movement program*, coinciding with the force vector of a steady amplitude and direction that changed tangentially with respect to the movement trajectory [17, 24]. In addition, the CC, estimated from the averaged EMG recorded in several repetitions of the same motor programs, was also shown to have a shape resembling slightly deformed force waves. Next, we normalize both waves, *E(t)* and *F(t)*, by setting their areas equal to unity; similarly, the length of the muscle *L(t)* will undergo the same normalization. As a result, an initial set of the time dependences $(E^0, F^0, L^0$; Fig. 1A) is transformed into the scaled set *(E, F, L)*, in which each function has the same area equal to unity (Fig. 1B). The normalized time functions *(E, F, L)* are defined at the time interval *[0, T]* by the scaling procedure:

$$E(t) = a_E E^0(t); a_E = \left[\int_0^T E^0(t)\,dt\right]^{-1};$$

$$F(t) = a_F F^0(t); a_F = \left[\int_0^T F^0(t)\,dt\right]^{-1};$$

$$L(t) = a_L\left[L^0(t) - L^0_{min}\right]; a_L = \left[\int_0^T \left(L^0(t) - L^0_{min}\right)dt\right]^{-1} \cdot \quad (4).$$

The L^0_{min} in Eq. (4) corresponds to a minimal value of the muscle length within the tested time interval (Fig. 1AI). Graphical results of the normalization procedure after calculating the scaling factors a_E, a_F, and a_L are shown in Fig. 1. For further modeling, we used pairs of the normalized dependences L_1, L_2; F_1, F_2, and E_1, E_2, in which indices *1* and *2* correspond to the shortening and lengthening movements, respectively. To compare CCs corresponding to opposite directions of the movement, we used the same scaling factor a_E that was defined for the shortening tests, always showing a greater integral intensity of EMG compared to the lengthening events. Therefore, areas under the E_2 curves after normalization are smaller than unity (Figs. 2DI and 5DI**)**. After performing

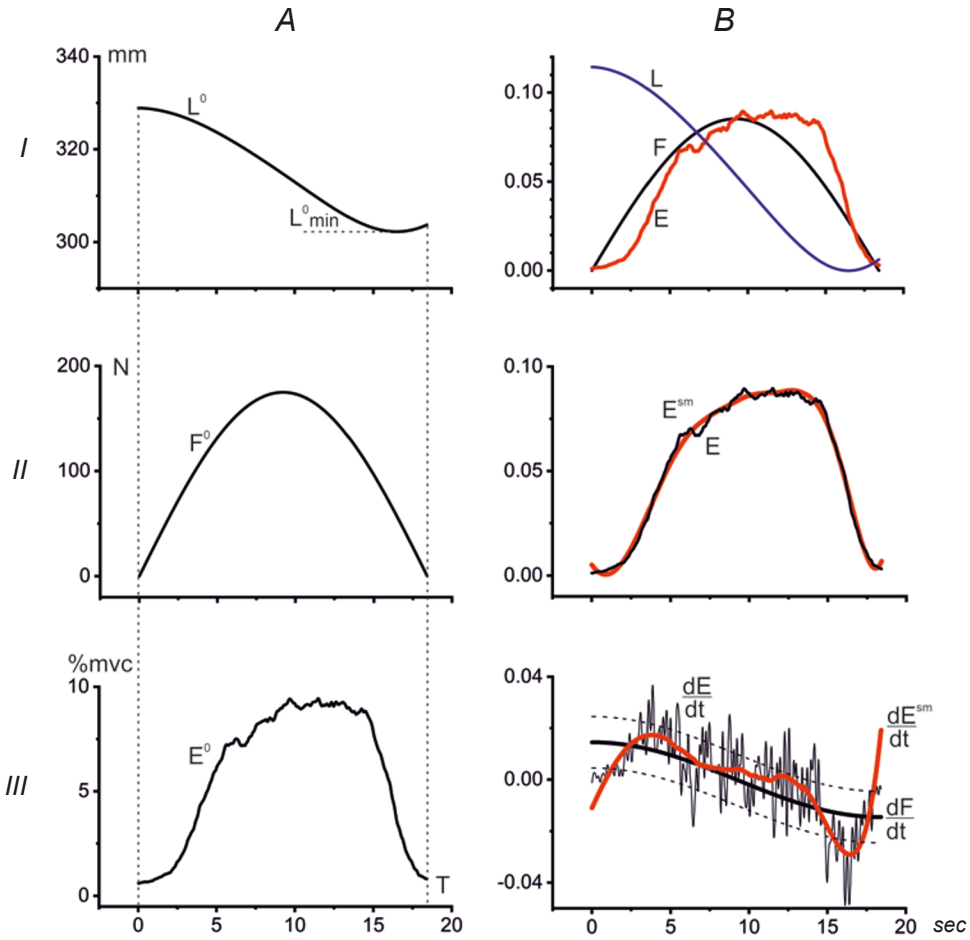

Fig. 1. Procedure of the data normalization. A) EMGs recorded from the *m. biceps brachii* (*BicBr*) of the subject with identified muscle geometry in tests with circular movements of his right hand within the plain passing via the shoulder joint [17]. The force wave developed by the muscle (F_0) and length changes of the latter (L_0) were calculated based on the positioning of the 3D printed bones of the tested subject [19]. The rectified and low-pass filtered surface EMG records were averaged for six repetitions of the identical movement tests. Details of the methods are described elsewhere [17, 25]. The averaged EMG record E_0 was calibrated in % of its intensity during the maximal voluntary contraction (MVC). B) Procedure of normalization (described in detail in the text). The corresponding normalized curves *F, L,* and *E* have the same areas equal to unity. Panel BIII presents a comparison of the time derivatives from *E(t)* records obtained with standard (300 p.p.t., Savitsky-Golay) and additional (500 p.p.t., Savitsky-Golay) smoothing procedures (black line *E*, and red line E^{sm} in panel BII). Dashed lines in panel BIII correspond to the range ±0.02 a.u. (arbitrary units) around the *dF/dt* dependency.

any mathematical procedure on the normalized functional dependences, it is possible to return to their original scales by inverse scaling.

T-model: analysis of the EMG pattern related to elbow flexion using a multiplicative correction procedure. After data normalization, we obtain a possibility for comparing shapes of the *E(t)* and *F(t)* functions, which are rather close to each other. Therefore, the original problem of finding a connection between functions F_0 and E_0 can be reduced to the analysis of the "distortion" of symmetric function *F* during its "transformation" (inverse) into an asymmetric function *E*. However, one can observe a similarity between changes in both functions if we compare their time derivatives $\frac{\partial E}{\partial t}$ and $\frac{\partial F}{\partial t}$ (Fig. 1BIII). This similarity becomes even more expressed when considering the derivative curve $\frac{\partial E^{sm}}{\partial t}$ obtained after a stronger smoothing procedure for *E(t)* (red curves in Fig. 1BII, III).

Assuming the closeness of the time derivatives $\frac{\partial E}{\partial t}$ and $\frac{\partial F}{\partial t}$ within the interval *[0, T]* and excluding edge effects, one can also verify that the derivative $\frac{\partial E}{\partial F}$ in Eq. (3) can be equated to unity. Taking this assumption into account

and integrating both sides of Eq. (3), we can transform it into the following integral form:

$$E(t) = F(t) - \int_0^t \frac{\partial F(\tau)}{\partial L(\tau)} \tilde{M}(\tau) V(\tau) d\tau, \qquad (5)$$

where $V(\tau) = \frac{\partial L}{\partial t}$ is the velocity of muscle length changes during a hand movement along the given trajectory; a correction factor $\tilde{M}(\tau)$ is introduced to compensate for distortions that might be connected, e.g., with the preceding assumption that $\frac{\partial E}{\partial F} = 1$.

Considering that the derivative $\frac{\partial F}{\partial L}$ in Eq. (5) coincides with the stiffness of muscle *S*, and renaming $\tilde{M}V = M$, we obtain the final form for the "transformation" of *F(t)* into *E(t)*:

$$E(t) = F(t) - \int_0^t S(\tau) M(\tau) d\tau, \; 0 \le t \le T. \qquad (6)$$

In accordance with Eq. (6), *E(t)* describes the change in time for the CC, which causes a given change in the muscle length *L(t)* simultaneously with the creation of a given force wave *F(t)* by the muscle (Fig. 2AI, CI). At the same time, Eq. (6) might be treated as a reverse process of some decomposition of the force wave *F(t)* with the help of the second integral term. Due to the normalization procedure used in the study, the integral term in

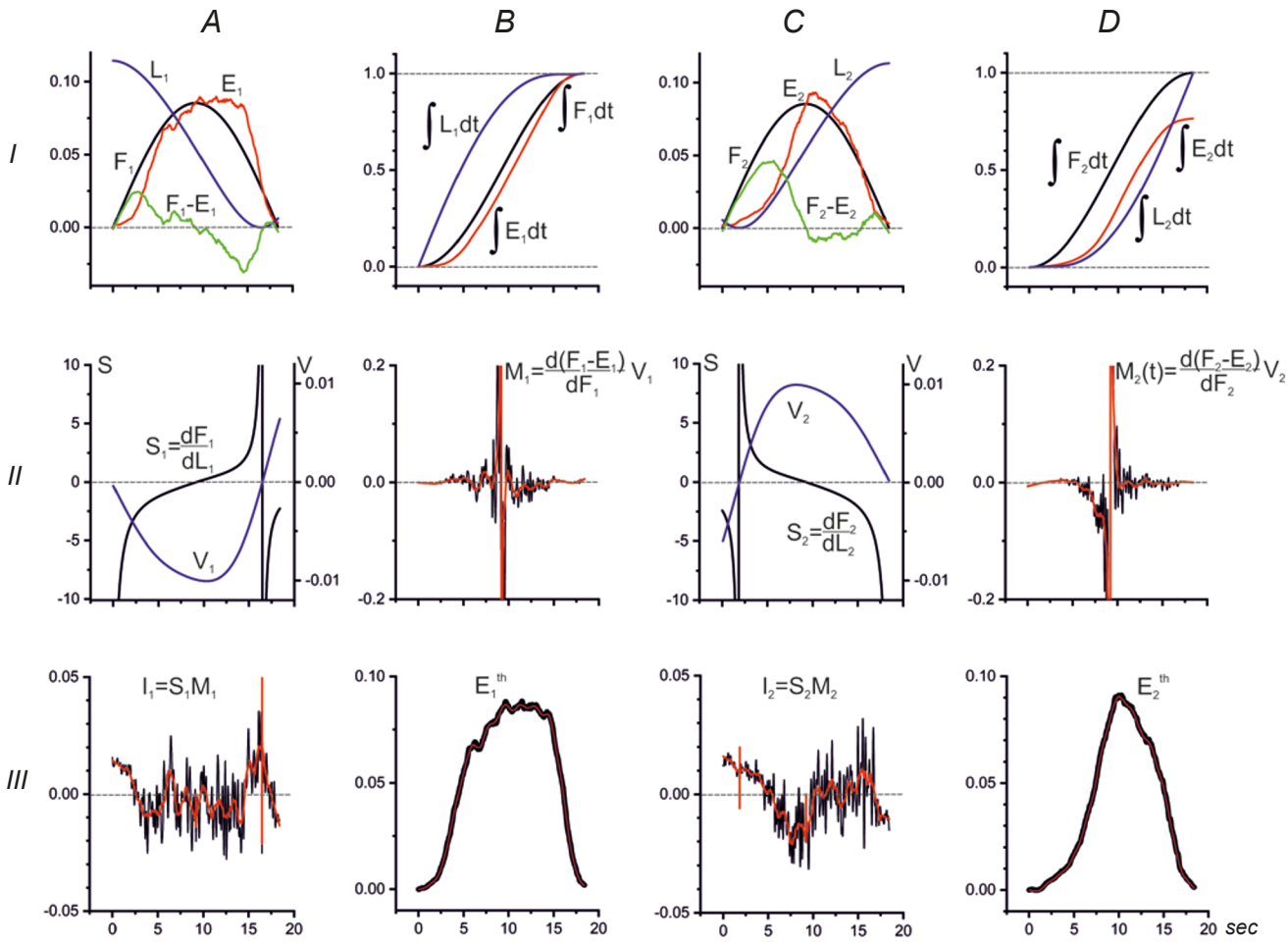

Fig. 2. T-model using the *multiplicative correction term*; modeling of the real experiment with the elbow flexor muscle *BicBr*. A–D) EMGs recorded in the shortening (A, B) and lengthening (C, D) movements were compared. Panels AI and CI contain superpositions of the normalized records of the force (*F*), EMG intensity (*E*), muscle length (*L*), and difference (*F–E*); indices *1* and *2* signify belonging of the respective parameters to shortening and lengthening directions of the movement, respectively. Elements of the normalization procedure are presented in panels BI and DI. Lines II and III illustrate the respective mathematical procedures described in the text. Calibration of the vertical axes is given in arbitrary units (a.u.) defined by the normalization procedure. In panels BII and DII, black lines describe the *multiplicative correction term M(t)* computed using the initial experimental *E(t)* records, including the 300-point Savitsky-Golay smoothing procedure; red lines correspond to the same computations using the additional 500-point smoothing of the above *E(t)* records (the E_1 record is shown in Fig. 1B). Two types of curves $E_{1,2}(t)$ were further used to compute $I_{1,2}$ and $E_{1,2}^{th}$ in line III.

Eq. (6) becomes equal to zero for the entire interval T, which determines the wave duration F(t):

$$\int_0^T S(\tau)M(\tau)d\tau = 0 \cdot \quad (7)$$

Therefore, the area of the regions of decreasing *E(t)* with respect to *F(t)* coincides with the area of regions where *E(t)* is greater (see the *F–E* curve in Fig. 2AI). However, Eq. (7) is valid only for the cases where areas of the normalized waves *E(t)* are equal to unity. Those, due to hysteresis effects, correspond mainly to the shortening trajectories (Fig. 2A, B). Application of the equal coefficients of normalization to the *E* waves in the shortening and lengthening movements belonging to the same experiment usually evoked a relative diminishing of the *E(t)* areas in the second case (Fig. 2C, D). In this case, a difference appears between the positive and negative values of the areas under the *F–E* curve; so, Eq. (7) does not hold.

The integrand in the integral term of Eq. (6) includes multiplication of the muscle stiffness *S(t)* and time-dependent correction term *M(t)*, which we will further call the *multiplicative correction term* (MCT). The MCT can be defined in two simple steps. First, we transform Eq. (7) as follows:

$$\int_0^t S(\tau)M(\tau)d\tau = F(t) - E(t). \quad (8)$$

Second, by differentiating the preceding expression and considering that $S(t) = \frac{dF(t)}{dL(t)}$, the MCT can be determined directly:

$$M(t) = \frac{d\left[F(t) - E(t)\right]}{dF(t)}V(t) \cdot \quad (9)$$

Circular movements of the hand with the parallel development of an accompanying force demonstrate the bell-shaped form of the forces created by both shoulder and elbow muscles [17]. This form of the force waves causes a change in the sign of the muscle stiffness at their tops; in shortening movements, it coincides with the transition from negative to positive (Fig. 2AII); reverse alternation of signs corresponds to lengthening movements (Fig. 2CII). The stiffness curves have essential discontinuities, the latter are located at the lower extreme points of the curves *L(t)* and, accordingly, at the zero points of the velocity curves *V(t)* (Fig. 2AII, CII). Similar discontinuities are also seen in the MCT curves (Fig. 2BII, DII), and they are located in correspondence with the *F(t)* apexes. The direction of the *M(t)* discontinuities is reversed with a change in the movement direction due to the respective dependency on the velocity (Fig. 2BII, CII). Due to the coincidence of the positions of zeros and discontinuities in the functions *S(t)* and *M(t)*, these discontinuities disappear after their multiplication in the integrand *I(t)=S(t)M(t)* (Fig. 2AIII, CIII). The smoothing procedure applied to *M(t)* records is shown by the red curves in Fig. 2BII, CII; using these curves for computing the integrands, *I(t)* is actually equivalent to similar smoothing at this stage (Fig. 2AIII, CIII). Finally, producing the final computation of the theoretical curves $E^{th}(t)$ for opposite movement directions, one can see a high-quality prediction of the CC waveforms by the T-model (Fig. 2BIII, DIII). Note a high extent of the coincidence of the predicted waveforms $E_{1,2}^{th}$ for the unsmoothed and smoothed records at the levels of computation of *M(t)* and *I(t)* signals. This coincidence shows that the integration procedure in Eq. (6) provides by itself a sufficient degree of signal smoothing.

T-Model for artificial test-signals. Figure 3 shows the signal conversion process described in the preceding for several types of the artificial signals that simulate possible time dependences of the difference *F(t)-E(t)*. Lines I and II show signals of sinusoidal forms of different amplitudes. Line I may be considered a model of the real records in Fig. 2, which are superimposed over the simulated curves. The panels relating to lines I and II show sinusoidal signals of different amplitudes. Line I, apparently, can be considered a model of real records in Fig. 2 superimposed on the simulated curves, whereas in line III, we consider symmetrical positioning of the difference signals using a set of the Gaussian curves with the same time parameters and different amplitudes. For all lines in Fig. 3, two normalized waveforms were used, sinusoidal *F(t)* and linearly dropping *L(t)* ones, rendering a constant negative velocity *V(t)* for the muscle length changes. The duration of these signals coincided with the duration of the above real muscle reactions shown in Fig. 2; thus, we were able to superimpose these records on sets of the corresponding artificial curves (red curves in line I). Some similarity between the red and black *F–E* curves (Fig. 3AI) can give us some general information about the model transformations of real and artificial signals. Essential discontinuities of the derivatives *d(F–E)/dF* within a middle time range are present only in both sinusoidal *F–E* signals, which are asymmetric and are absent in the symmetrical input signals modeled by the Gaussian curves (Fig. 3B). After multiplying the MCT by the stiffness, the

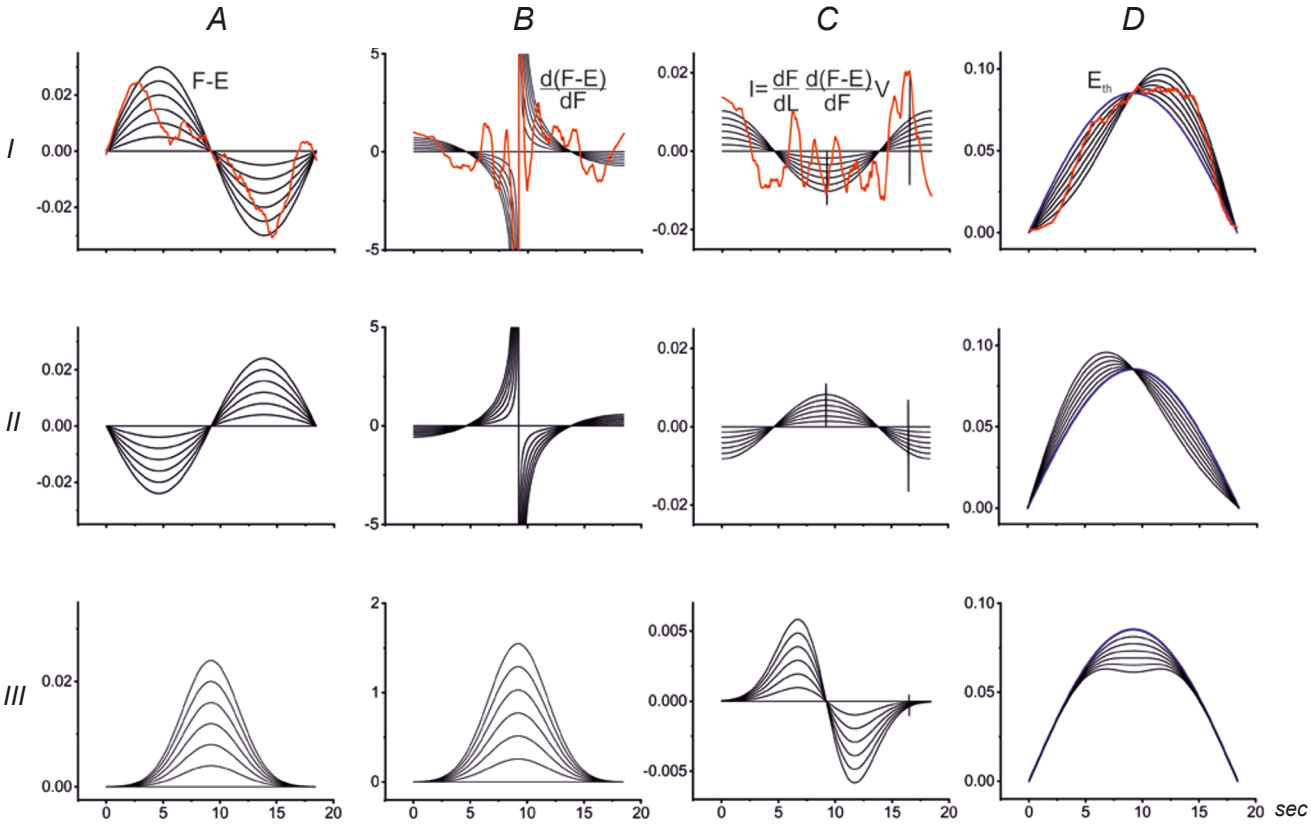

Fig. 3. Testing of the T-model with artificial *F–E* signals, sinusoidal (lines I, II) and Gaussian (line III). A–D) Calculation procedures are the same for all test signals, as indicated in line I. The corresponding real records from the experiment shown in Fig. 2A, B are also superimposed on line I (red lines).

discontinuities in the integrands of Eq. (6) disappear (Fig. 3CI, II). The final calculation of the theoretical E^{th} curves shows the same asymmetry as in the real EMG records, showing a lag in both phases of the force change (Fig. 3DI). The reverse order of the *F–E* sinusoids causes a phase advance of the CCs (Fig. 3DI), while symmetrical input signals also correspond to symmetrical CC responses.

Gaussian fitting procedure in the T-model. Figure 4 clearly shows that real *F–E* curves usually contain several wave components of different amplitudes and durations. To visualize the signal conversion process described previously at different stages, we tried to smooth the original *F–E* curves before running the main computations. Using the Gaussian curves in the fitting procedure greatly simplifies this process and makes it quite clear. Four or five Gaussian curves ($G_{1,2}^{\ i}$ in Fig. 4CI) are usually well suited for a satisfactory fit of the CC curves. Firstly, the position and amplitudes of the individual Gaussian components were chosen by eye in such a way that they corresponded to the most pronounced peaks of the signals under study. Then, the curves representing a sum of the components ($G_1=\sum G_1^i$; $G_2=\sum G_2^i$ in Fig. 4DI) were superimposed on the original signals. By varying the amplitude, width, and position of the constituent Gaussian components $G_{1,2}^{\ i}$, it was usually possible to achieve the satisfactory agreement between these curves and original *F–E* curves in several iterations. Computation of the MCT and integrand in Eq. (6) does not differ from the previously described ones; therefore, the theoretically defined corresponding E^{th} and $E^{th}(G)$ curves are well suited to each other (Fig. 4, line III). The software used in this study allows us to observe the evolution of the E^{th} curves and the wave components in the integrands in Eq. (6) as the parameters of the Gaussian waves change, thus gaining an idea of a possible influence of the various wave components of the *F–E* curves on the E^{th} curves. For example, we can observe how small changes in various Gaussian waves (central position, amplitude, and width), which model the shapes of the *F–E* curves, cause corresponding changes in the overall shape of E^{th}. When comparing the integrands of Eq. (6) calculated for Gaussian approximations of

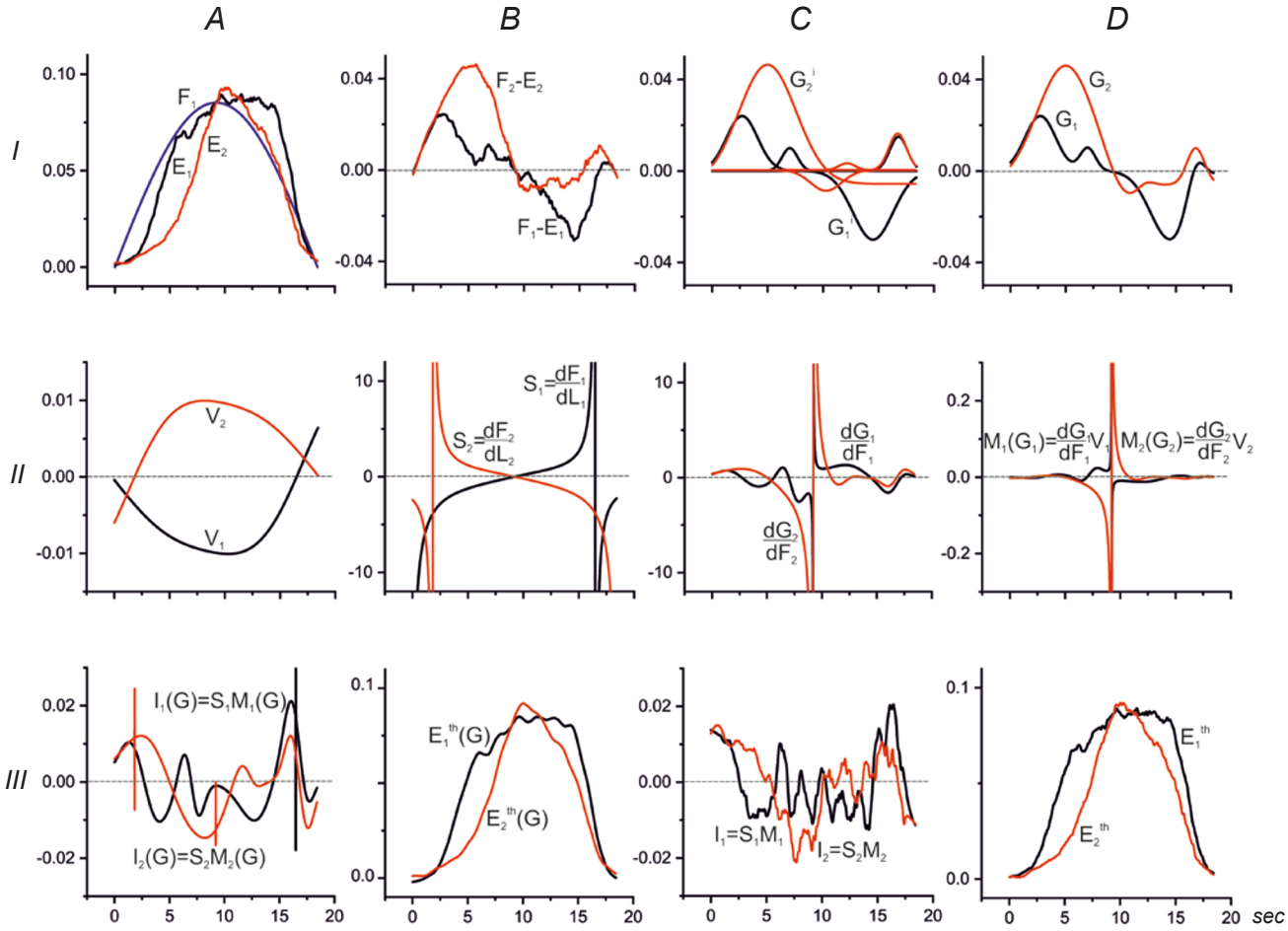

Fig. 4. Gaussian approximation of the signals in the T-model. A) Superposition of the normalized signals under study, which were earlier presented in Fig. 2A, C; the differences $F_{1,2}$–$E_{1,2}$ are shown in B). Sum of four Gaussian components ($G_{1,2}^{i}$) (C, D) provides an approximation of the *F–E* differences used for modeling the central commands $E_{1,2}^{th}$. Lines II and III show the successive stages of modeling with the approximated *F-E* differences $G_{1,2}$; the $I_{1,2}$ and $E_{1,2}^{th}$ records obtained with the approximated and original *F-E* records are compared in line III.

the *F–E* curves and their direct analogs (Fig. 4AIII, BIII), the approximated reactions are somewhat simpler and do not look like smoothed copies of the original curves. The simulated Gaussian records include approximately three–four distinct oscillations compared to seven to nine ones in the original records. At the same time, the most important parts of the integrands, which belong both to their original entries and to the corresponding Gaussian approximations, are associated with waves of the greater amplitudes at the beginning and end. The first large waves in the $I_2(G)$ and I_2 records (red lines in Fig. 4AIII, BIII) provide a more pronounced and durable lag between the $E_2(G)$ and E_2 curves compared to the $E_1(G)$ and E_1. In contrast, at the end of the force action interval, such a lag becomes more clearly expressed in curves $E_1^{th}(G)$ and E_1^{th}, so that the corresponding waves in integrands $I_1(G)$ and I_1 become more distinct compared to $I_2(G)$ and I_2, respectively.

T-model: analysis of the EMG pattern related to elbow extension. In our previous experimental paper [17], a great diversity in the CCs coming to different muscles of the elbow and shoulder joints was demonstrated. Slightly different EMG responses are observed in the elbow extensors and shoulder muscles when compared to the preceding example of the elbow flexors. For EMG responses of the extensors of the elbow joint, a more pronounced difference can be noted between the records associated with the movements of muscle shortening and lengthening evidenced by Fig. 5, which shows the response of the elbow extensor muscle *triceps longus* (*TricLg*) recorded in the same experiment as the responses of the elbow flexor *BicBr* in Figs. 1, 2, and 4. A more pronounced difference between

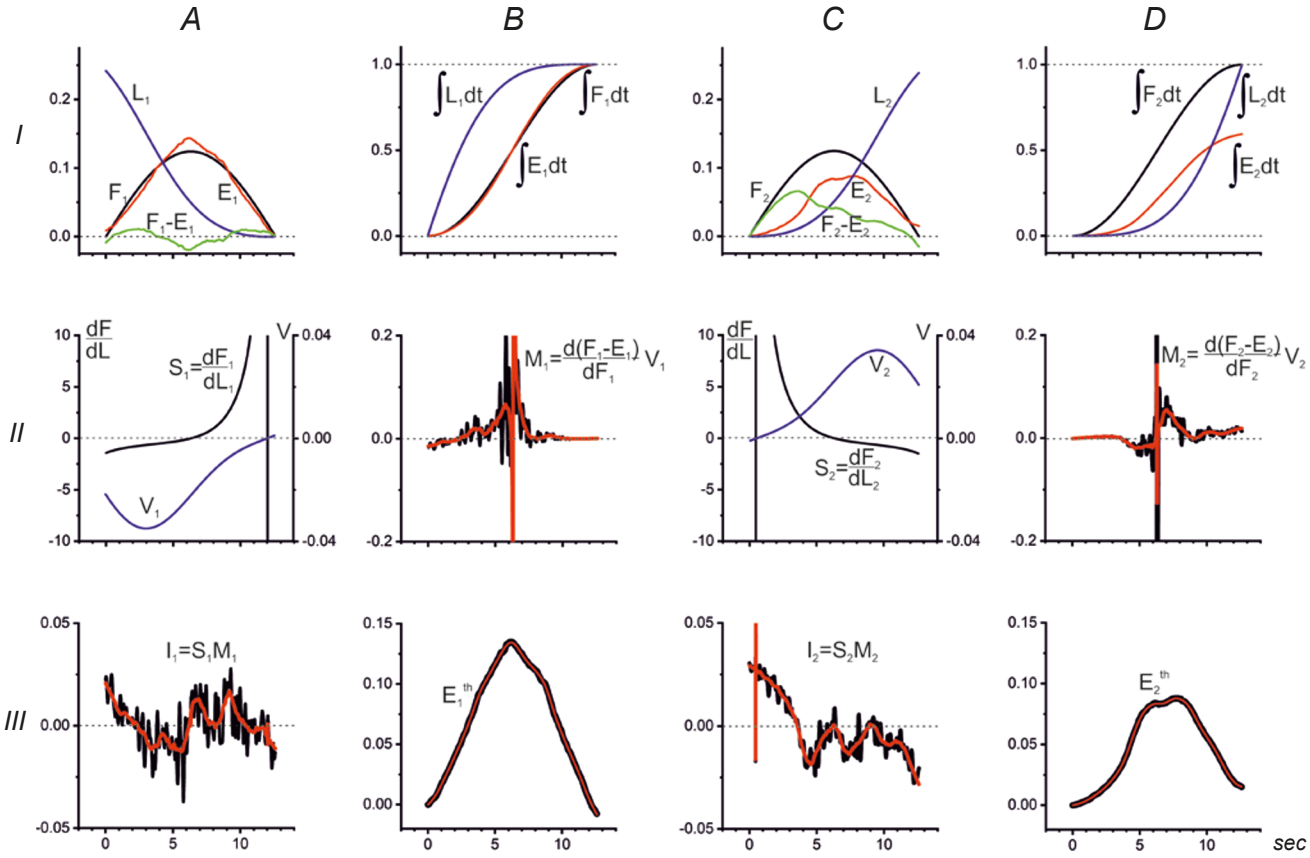

Fig. 5. T-model with real EMG records from the elbow extensor *m. triceps long* (*TricLg*). The EMGs are compared during shortening (A, B) and lengthening (C, D) movements; the presentation scheme, colors, and designations are shown in Fig. 2.

the CCs corresponding to muscle shortening and lengthening is seen when comparing the areas under the E_2 curves in the *BicBr* and *TricLg* reactions. (Figs. 2DI and 5DI). At a rising phase of the force in the shortening movements, the *TricLg* muscle demonstrates almost a complete absence of the time lags, which, however, clearly appeared in the respective lengthening traces (compare pairs of the traces E_1, F_1 and E_2, F_2 in Fig. 5AI, DI). The proposed procedure of the $E(t)$ restoration based on Eq. (6) works quite satisfactorily, and theoretically defined $E^{th}(t)$ traces are not sensitive to high-rate signal oscillations at various stages of computations. Such oscillations are clearly seen if an additional filtering procedure is applied at the stage of the MCT computations (red lines in Fig. 5BII, DII). Further calculation of the integrands in the integral parts of Eq. (6) for the smoothed and original MCT retains the common features of such a difference (Fig. 5AIII, DIII), which almost disappears at the final stage of determining E^{th} (Fig. 5A–D, line III). Considering shapes of the filtered integrands (Fig. 5AIII), it should be noted that a "triangled" shape of the CCs, which sometimes is encountered in EMG responses of the elbow extensors and both flexors and extensors of the shoulder [17], may be connected with rather durable sections (3–4 sec) of an almost linear drop of the integrands. However, a noticeable curvature of the growing part of the CCs with an expressed lag in relation to the force curves (Fig. 5DIII) corresponds to the oppositely directed curvature of the corresponding parts of the integrands.

T-model using the additive correction procedure. The whole process of converting waves $F(t)$ into $E(t)$ includes a chain of the basic steps for calculating the muscle stiffness $S(t)$ and MCT, $M(t)$, as well as their multiplication $S(t)M(t)$ in the final calculation by Eq. (6). Figures 2 (lines II and III) and 5 (lines II and III) demonstrate these event chains for the respective real signals. The essential discontinuities that are present at the $S(t)$ and $M(t)$ records after the respective differentiation procedures, coincide with zeroes of each other; therefore, after multiplication of these components in the integrands, $I(t)=S(t)M(t)$, the discontinuities

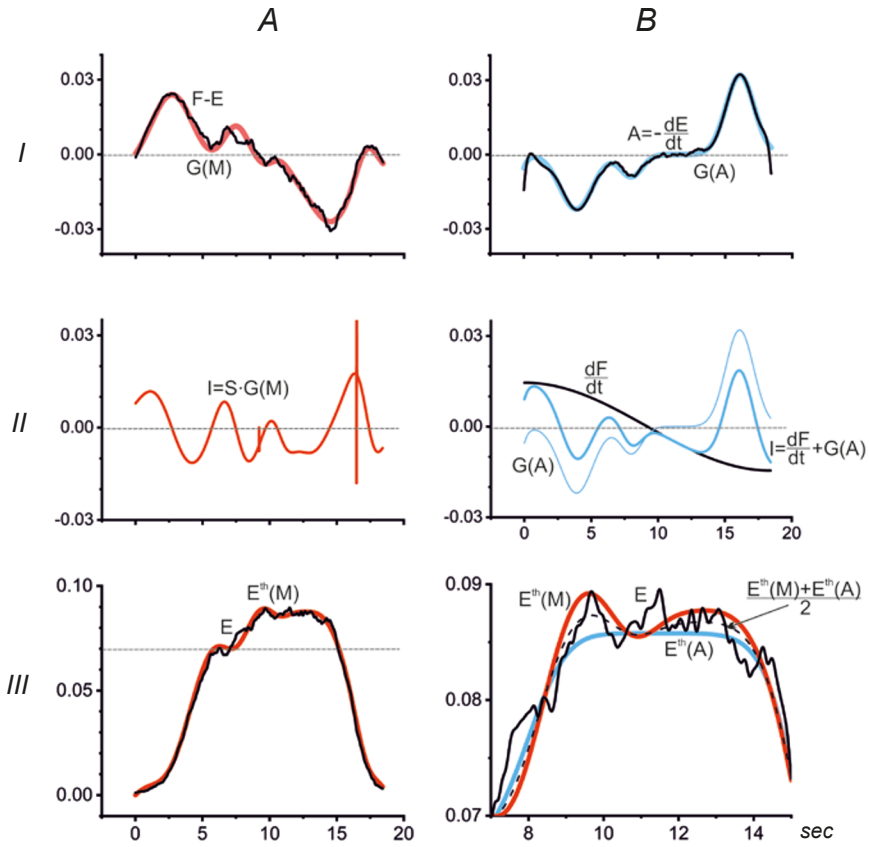

Fig. 6. Comparison of T-models using the *multiplicative* and *additive correction methods*. A and B) Gaussian approximations are applied to the input signals of the *multiplicative* (M) and *additive* (A) *correction terms*, and the respective curves are lighted by red and blue colors. The $E^{th}(M)$ and $E^{th}(A)$ curves resulting from the simulation are shown in panel BIII, which also shows the result of their joint averaging.

disappear. However, when considering the sets of normalized parameters *(F, L, E)*, the range of changes of the integrands in Eq. (6) constitutes only several hundreds, whereas the muscle stiffness is changed by a several hundred times wider range (Figs. 2 and 5). Thus, *S(t)* and *I(t)* vary within different limits; so, *M(t)* cannot be considered an element of any corrective procedure that only slightly changes muscle stiffness. Therefore, if we, instead of the preceding multiplicative correction, consider some kind of additive correction, the object of correction must be changed in comparable limits as the already defined integrand *I(t)*. The force velocity $\frac{dF(t)}{dt}$ covers exactly the same range as the integrand in Eq. (6) (Fig. 6BII). Therefore, by analogy with Eq. (6), introducing *an additive correction term* (ACT), *A(t)*, we can consider the following expression:

$$E(t) = F(t) - \int_0^t \left[\frac{\partial F(\tau)}{\partial \tau} + A(\tau) \right] d\tau, \qquad 0 \le t \le T. \quad (10)$$

Similarly to the previously described procedure, Eq. (10) is transformed into the following form:

$$\int_0^t \left[\frac{\partial F(\tau)}{\partial \tau} + A(\tau) \right] d\tau = F(t) - E(t). \quad (11)$$

Differentiating both sides of Eq. (11), *A(t)* can be determined directly:

$$A(t) = -\frac{\partial E(t)}{\partial t}. \quad (12)$$

The preceding two methods of theoretical reconstruction of the force traces *F(t)* into the CCs $E^{th}(t)$ are compared in Fig. 6. Columns A and B describe the calculations by Eqs. (6) and (10), respectively. In both cases, we applied Gaussian approximation of the input signals; therefore, *G(F–E)* was further used in the first method, while *G(A)* was used in the second method (Fig. 6, line I). The corresponding curves that determine the integrands in Eqs. (6) and (10) (Fig. 6, line II), despite their similarity, also cause the resulting dependencies $E^{th}(M)$ and $E^{th}(A)$ to diverge. Joint averaging of the

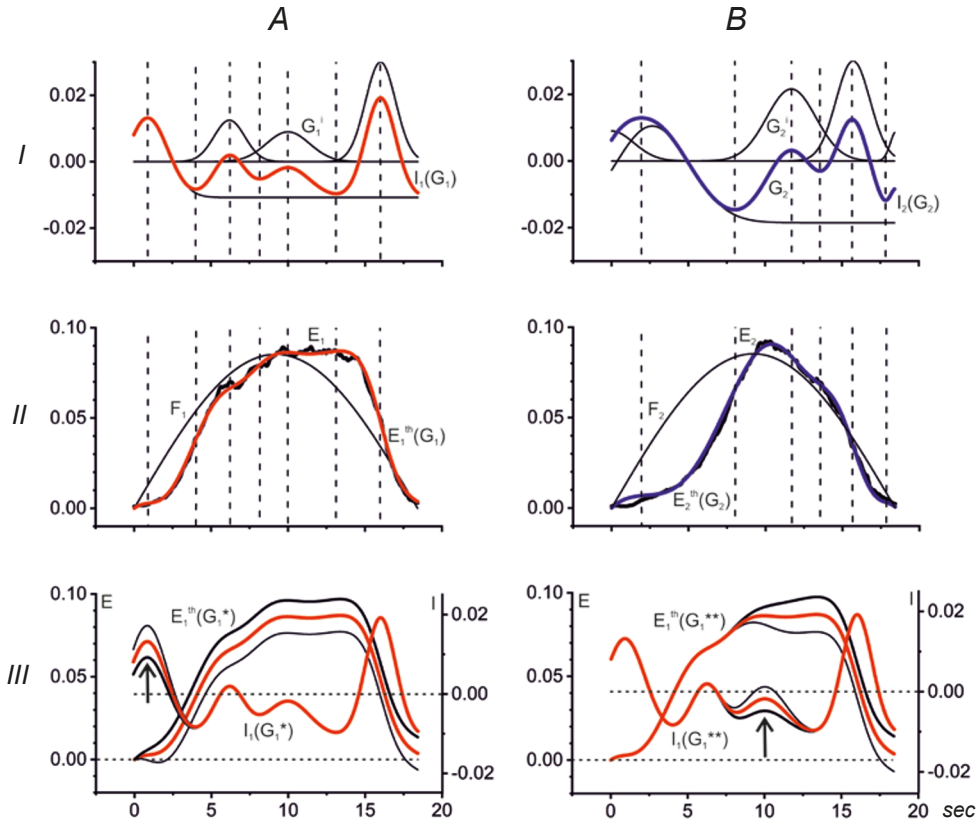

Fig. 7. Gaussian fitting of the integrands in the *multiplicative correction procedure*. A and B) Sum of the four (A) and five (B) Gaussian components ($G_{1,2}^{i}$) was used for additional fitting procedure applied to the earlier calculated integrands $I_1(G)$ and $I_2(G)$, which are shown in Fig. 4AIII. The corresponding curves modeling the EMG activity related to opposite directions of the movements are highlighted in color; red and blue lines correspond to the tests with predominant muscle shortening and lengthening, respectively; original EMG records are shown in line II by thick black lines. A procedure of "manual" selection of the parameters of the Gaussian curves ($G_{1,2}^{i}$), the sum of which ($G_{1,2}$) provides an almost perfect match of the model ($E_{1,2}^{th}$) and experiment ($E_{1,2}$). Line III demonstrates results of the amplitude changes of the first and third Gaussian components in G_1 (shown by arrows). The optimal and "artificially shifted" reactions are shown by red and black (thick, thin) lines. Note a correspondence between the thick and thin lines in I_1 and E_1^{th} in line III. Vertical dashed lines in panels with lines I and II indicate the extrema points of I_1 and I_2.

two methods can improve the quality of the resulting model prediction (Fig. 6BIII).

Manual fitting of the integrands in the integral term of the T-model. The quality of CC prediction by the T-model after preliminary Gaussian approximation of the *P–E* curves (Fig. 4) even improves somewhat if a similar "manual" approximation procedure is repeated for the integrands themselves (Fig. 7).

The fitting procedure in this case, as is shown in Fig. 7 (line III), turned out to be very sensitive to changes in the amplitudes of individual Gaussian components. Such changes cause stationary shifts of the simulated *E*-curves within the remaining time of the test, even after termination of their action inside the locally changed integrands *I(G)*. These interrelated changes in the *I(G)* and *E(G)* signals may demonstrate a fine tuning of the fitting procedure. Vertical dashed lines pointing out extrema points along the integrand curves can help us to visualize the action of local waves in the integrand signals on respective turnings of the resulting E^{th} curve. This can be especially useful when modeling processes are performed under conditions of incomplete information about biomechanical constraints.

T-model under changing force waves. The experimental data presented in this study were obtained using a setup that allowed us to change the force waves in the biofeedback mode and to simultaneously leave the trajectory and velocity of the movement itself unchanged. Such experiments should be carried out in the future; here, we consider only their possible analysis (Fig. 8). If the *F*-wave is summed with small sinusoidal signals having the same period as its duration, then the resulting signals will show a smooth deformation, shifting

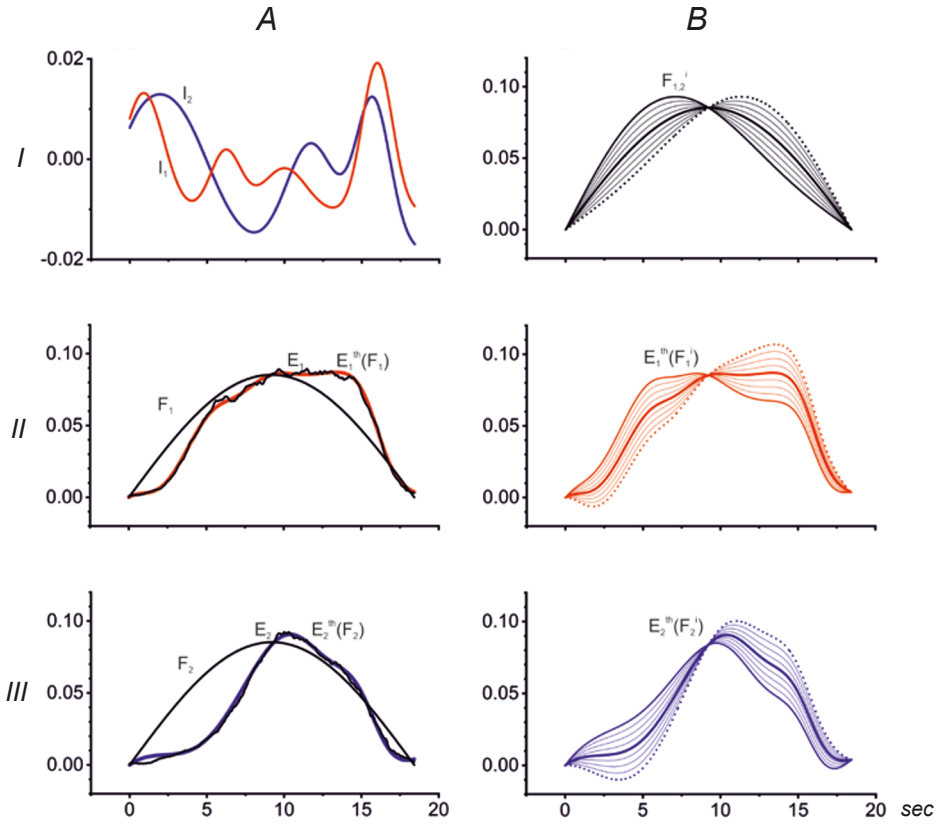

Fig. 8. Theoretical modeling of the force wave modification. A) Plots of the normalized *F* and *E* waves and their theoretical approximation by Eq. (6) (records $I_{1,2}$, $F_{1,2}$, and $E_{1,2}$ are taken from Fig. 7). B) Sets of the modeled curves, $F_{1,2}^i(t)=F_{1,2}(t) + i0.01sin(2\pi t/T)$, T is the duration of the force wave; $-4 \le i \le 4$; $E_{1,2}^{th}(F_{1,2}^i)$ are defined by Eq. (6) provided that the integrand dependencies $I_{1,2}$ (panel AI) are not changed.

their maxima to the left or to the right, depending on the amplitude and sign of the sinusoidal components (Fig. 8BI). Areas of the new force waves will not change, thus satisfying the normalization conditions given by Eq. (4). In view of the fairly close correspondence between the normalized *E* and *F* waveforms, it might be assumed that areas of the modified $E+\delta E$ waves will also not change significantly, demonstrating the same shifting trends as those of the $F+\delta F$ waves. If we then try to calculate the transformed waves $E+\delta E$ according to Eq. (6), then, in the first approximation, one can assume that the integrands $I_{1,2}$ (Fig. 8AI) will remain unchanged, since they are based on the difference $F–E$; therefore, supposedly very similar additions δF and δE can cancel each other out. The results of the modeling are shown in Fig. 8B as the sets of the curves $E_1^{th}(F_1^i)$ and $E_2^{th}(F_2^i)$. Such a model can serve as a prerequisite for further experimental analysis based on incomplete biomechanical information. Small changes in the force commands in association with a stable passive movement program make it possible to clarify at least part of the biomechanical limitations associated with this motor task.

DISCUSSION

This study is a further development of a "thermodynamic" approach [14], which is designed to model the functional relationship between the CCs coming to the muscle and the mechanical parameters defining its contraction. It is quite clear that, within the framework of the given experimental approach, complete information cannot be obtained about the activation patterns for all muscles participating in a given movement program. First, the recorded EMG activity depends both on the position of the electrodes and on some recording conditions; in addition, it is also practically impossible to obtain records from deeply located muscles; moreover, the redistribution of activity between synergists and their interaction with antagonists may create additional undefined influences (for a review, see

[23]). However, information on temporal changes in the muscle length and force may also be unavailable or incomplete in most cases. Nevertheless, it seems that it is possible to speak about a definite progress in getting biomechanical information, at least for the experimental data served for modeling in the present study. In this study, a new methodical approach to the movement tests was used, which included a complete separation of the movement itself from the process of force generation. The movement trajectory becomes highly accurate, and it is created by a digitally controlled mechatronic device; thus, it is sufficient for the subject to follow a preprepared force generation program in biofeedback mode; the method provides an exact correspondence between the force and positioning along the movement trace [24]. Additionally, preliminary MRI identification of the bones under study has been carried out and followed by their 3D printing, which makes it possible to determine the positions of the origin and insertion points of the muscle tendons [19], improving the accuracy of temporal reconstruction of the muscle length and force trajectories.

This modification of the T-model is devoted to the consideration of circular movements of the hands, when flexors and extensors of the elbow and shoulder joints create successive force waves resembling symmetrical segments of the sinusoidal signals [17, 25]. The sum of the forces developed by individual muscles creates a resultant force in the area of the hand, which is directed tangentially to the circular trajectory of the movement. The forms of averaged EMGs in synergistic muscles belonging to each of the joints often have been shown to have fairly close profiles usually differing from each other mainly in their intensity. In the same way, one can notice a certain similarity in forms of the force and EMG waves in each of the studied muscles. To compare and analyze the shapes of the studied signals, i.e., signals *F(t), L(t)*, and *E(t),* we proposed a procedure for their normalization that consists of equalizing the time integrals of equal duration coinciding with that of the force wave. After any mathematical procedures, models with normalized signals easily return to their original scales. Normalizations make it possible to reformulate our initial consideration of the problem when the signals *F(t)* and *E(t)* were considered in their real scales. Finally, the problem is to obtain information about *E(t)* based on the waveform *F(t)* and a corrective integral component, which should contain some preliminary evaluation of possible changes in the following force derivatives, $\frac{dF(t)}{dL(t)}$ (muscle stiffness) or $\frac{dF(t)}{dt}$ (rate of the force change). In these cases, the MCT and ACT methods are applied. In both cases, the correction terms use information about the *E(t)* waveform in its derivatives $\frac{dE}{dF}$ (MCT) and $\frac{dF}{dt}$ (ACT). Within the framework of the approach used, these derivatives are determined directly, but for an unknown finite configuration of *E(t)*, it is necessary to make preliminary assumptions. The most informative sections are found at the beginning of the rising front of the force wave and in the middle part of its falling branch, where tendencies of delay or advance between the signals *E(t)* and *F(t)* are formed. We have also noticed that the best results of fitting may be achieved by simultaneous application of the preceding methods by averaging the reconstructed CC models.

Various types of the test signals seem to be useful for considering basic principles of the input–output relationships in the system under study (Fig. 3). The use of sinusoidal or Gaussian signals for testing shows the features of the formation of "lagging" and "leading" types of the CC to provide a symmetrical bell-shaped force signal at the output of the system. Using a Gaussian approximation is probably the most convenient way to compare different types of the CCs, which correspond to identical force profiles in oppositely directed movements (Fig. 4). The Gaussian models allow us to easily compare differences at the rising and falling branches in the modeled CCs. The differences are most pronounced when the integrands in the corresponding integral terms are compared regarding the shortening and lengthening movements (Fig. 4AIII).

As our study is based on the analysis of stationary configurations of length and force trajectories, the T-model may, thus, look somewhat trivial, since its integral component contains information about the difference between the input and output signals. At the same time, the integrand in the multiplicative version of the correction (see Eqs. (7) and (8)) contains important mechanical characteristics of the muscle in a given movement program, such as the stiffness and rate of change in the length. We cannot vary these parameters in the existing experimental data selected for model testing. However, it is likely that some important information for the modeling process might also be obtained from small changes in the movement trajectories, such

as their positioning in the operating space or velocity variations. The same is concerned with changes in the force trajectories, which can be provided by varying biofeedback programs of the force generation. We can also assume that, for the present model approach, a reverse task relating to reconstruction of the unknown mechanical variables, i.e., the muscle force and/or length, based on the direct EMG records is of a definite interest.

In the present study, rather slow movements were used for the tests (Fig. 1AI, the maximum speed of muscle contraction did not exceed 2.5 mm/sec), which corresponded to a range of the so-called quasistatic movements [26]. At the same time, the force generation process is difficult to treat within the framework of the equilibrium point hypothesis proposed by Anatol Feldman [26, 27], apparently due to strong hysteretic properties of the active muscle, both by itself (under conditions of artificial stimulation) and when it is included in the spinal and long-loop reflex circuits (for a review, see [21, 23]). Comparison of different directions of circular movements demonstrates statistically significant differences in CCs to both elbow and shoulder muscles [17].

Our present study is, therefore, devoted to further development of the "thermodynamic" model (T-model) in its application to the analysis of our "fresh" experimental data describing the time profiles of the CCs coming to the arm muscles during circular movements of the hand. Initially, the T-model was based on equations that determine the relationship between infinitesimal changes in main parameters of the movement, E (EMG intensity, or CC), F (muscle force), and L (muscle length), which, by an analogy with classical thermodynamics, are considered exact differentials. At present, the T-model is supplemented with a procedure for rescaling the indicated parameters by aligning their time integrals within intervals of the force action. To determine the integrands in the integral components of the corresponding T-models, we chose multiplicative and additive correction conditions applied to muscle stiffness and force velocity, respectively. The Gaussian approximation in the T-model is assumed to be capable of being especially effective when the available information is limited by the EMG data, and the biomechanical status of the movement can only be predicted in advance.

This is mostly a theoretical study using earlier obtained experimental data. All persons involved in additional motor tests and the person subjected to MRI examination gave their informed written consent. Thus, this study complies with the existing international ethical requirements for works of this kind, which was confirmed by the Ethical Committees of the Bogomolets Institute of Physiology and the Gdańsk University of Physical Education and Sports.

The authors, A. I. Kostyukov, A. V. Gorkovenko, A. V. Maznychenko, and I. V. Sokolowska, confirm the absence of any conflicts over commercial or financial relations, relations with organizations or individuals that could in any way be related to the study, and also in interrelations between the co-authors.

REFERENCES

1. N. A. Bernstein, *The Coordination and Regulation of Movements*, London: Pergamon Press; 1967.
2. C. B. Hart and S. F. Giszter, "Modular premotor drives and unit bursts as primitives for frog motor behaviors," *J. Neurosci.*, **24**, No. 22, 5269–5282 (2004); doi: 10.1523/JNEUROSCI.5626-03.2004.
3. P. Saltiel, K. Wyler-Duda, A. D'Avella, et al., "Muscle synergies encoded within the spinal cord: evidence from focal intraspinal NMDA iontophoresis in the frog," *J. Neurophysiol*., **85**, No. 2, 605–619 (2001); doi: 10.1152/jn.2001.85.2.605.
4. M. C. Tresch, V. C. Cheung, and A. d'Avella, "Matrix factorization algorithms for the identification of muscle synergies: evaluation on simulated and experimental data sets," *J. Neurophysiol.*, **95**, No. 4, 2199–2212 (2006); doi: 10.1152/jn.00222.2005.
5. M. C. Tresch and A. Jarc, "The case for and against muscle synergies," *Curr. Opin. Neurobiol.*, **19**, No. 6, 601–607 (2009); doi: 10.1016/j.conb.2009.09.002.
6. S. A. Safavynia, G. Torres-Oviedo, and L. H. Ting, "Muscle synergies: implications for clinical evaluation and rehabilitation of movement," *Top. Spin. Cord Inj. Rehabil.*, **17**, No. 1, 16–24 (2011); doi: 10.1310/sci1701-16.
7. E. Bizzi and V. C. K. Cheung, "The neural origin of muscle synergies," *Front. Comput. Neurosci*., **7**, 51 (2013); doi: 10.3389/fncom.2013.00051.
8. M. L. Latash, "Laws of nature that define biological action and perception," *Phys. Life Rev.*, **36**, 47–67 (2021); doi: 10.1016/j.plrev.2020.07.007.
9. A. d'Avella and F. Lacquaniti, "Control of reaching movements by muscle synergy combinations," *Front. Comput. Neurosci.*, **7**, 42 (2013); doi: 10.3389/fncom.2013.00042.
10. A. d'Avella, A. Portone, L. Fernandez, and F. Lacquaniti, "Control of fast-reaching movements by muscle synergy combinations," *J. Neurosci.*,. **26**, No. 30, 7791–7810 (2006); doi: 10.1523/JNEUROSCI.0830-06.2006.

11. D. J. Berger, R. Gentner, T. Edmunds, et al., "Differences in adaptation rates after virtual surgeries provide direct evidence for modularity," *J. Neurosci.*, **33**, 30, 12384–12394 (2013); doi: 10.1523/JNEUROSCI.0122-13.2013.
12. T. I. Abramovich, I. V. Vereshchaka, A. M. Tal'nov, et al., "Coordination of activity of the shoulder belt and shoulder muscles in humans during bimanual synchronous two-joint movements," *Neurophysiology*, **47**, 310–321 (2015); doi: 10.1007/s11062-015-9538-6.
13. A. I. Kostyukov, "Theoretical analysis of the force and position synergies in two-joint movements," *Neurophysiology*, **48**, No. 4, 287–296 (2016); doi: 10.1007/s11062-016-9601-y.
14. A. I. Kostyukov. "A "thermodynamic" model of central commands coming to the muscles during upper limb movements," *Neurophysiology*, **51**, 366–380 (2019); doi: 10.1007/s11062-020-09830-z.
15. T. Tomiak, T. I. Abramovych, A. V. Gorkovenko, et al., "The movement- and load-dependent differences in the EMG patterns of the human arm muscles during two-joint movements (a preliminary study)," *Front. Physiol.*, **7**, 218 (2016); doi: 10.3389/fphys.2016.00218.
16. A. I. Kostyukov, O. V. Lehedza, A. V. Gorkovenko, et al., "Hysteresis and synergy of the central commands to muscles participating in parafrontal upper limb movements," *Front. Physiol.*, **10**, 1441 (2019); doi: 10.3389/fphys.2019.01441.
17. A. I. Kostyukov, A. V. Gorkovenko, Y. A. Kulyk, et al., "Central commands to the elbow and shoulder muscles during circular planar movements of hand with simultaneous generation of tangential forces," *Front. Physiol.*, **13**, 864404 (2022); doi: 10.3389/fphys.2022.864404.
18. S. Israely, G. Leisman, and E. Carmeli, "Neuromuscular synergies in motor control in normal and poststroke individuals," *Rev. Neurosci.*, **29**, No. 6, 593–612 (2018); doi: 10.1515/revneuro-2017-0058.
19. A. V. Gorkovenko, S. S. Strafun, Y. A. Kulyk, et al., "Motor commands for planar movements of the upper limb: modeling with taking into account realistic osteo-muscular relations," *Neurophysiology*, **52**, No. 3 222–233 (2020); doi: 10.1007/s11062-020-09874–1.
20. A. I. Kostyukov, "Muscle dynamics: dependence of muscle length on changes in external load," *Biol. Cybern.*, **56**, No. 5–6, 375–387 (1987); doi: 10.1007/BF00319517.
21. A. I. Kostyukov, "Muscle hysteresis and movement control: a theoretical study," *Neuroscience*, **83**, 303–320 (1998); doi: 10.1016/s0306-4522(97)00379-5.
22. G. B. Thomas Jr. and R. L. Finney, *Calculus and Analytic Geometry* (9th ed.), Addison-Wesley: 1996. ISBN: 978-0201531749, 0201531747.
23. A. I. Kostyukov, *Dynamic Properties of the Motor System of Mammals*, Kyiv, FADA Ltd, 2007.
24. M. Zasada, A. V. Gorkovenko, S. S. Strafun, et al., "A new approach to the study of two-joint upper limb movements in humans: Independent programming of the positioning and force," *Neurophysiology*, **52**, 397–406 (2020); doi: 10.1007/s11062-021-09896-3.
25. A. I. Kostyukov and T. Tomiak, "The force generation in a two-joint arm model: analysis of the joint torques in the working space," *Front. Neurorobot.*, **12**, 77 (2018); doi: 10.3389/fnbot.2018.00077.
26. A. G. Feldman, "Space and time in the context of equilibrium-point theory," *Wiley Interdiscip. Rev.: Cogn. Sci.*, **2**, No. 3, 287–304 (2011); doi: 10.1002/wcs.108.
27. A. G. Feldman, "Active sensing without efference copy: referent control of perception," *J. Neurophysiol.*, **116**, No. 3, 960–976 (2016); doi: 10.1152/jn.00016.2016.